Research Paper

Investigation of Seismic Stress Changes in the Makran Subduction Zone

Mehrdad Mostafazadeh[1*] and Leila Mahshadnia[2]

1. Assistant Professor, Seismological Research Center, International Institute of Earthquake Engineering and Seismology (IIEES), Tehran, Iran, *Corresponding Author; email: mehrdad@iiees.ac.ir
2. Research Expert, Institute of Seismology, International Institute of Earthquake Engineering and Seismology (IIEES), Tehran, Iran

Received: 21/09/2022
Revised: 05/11/2022
Accepted: 31/12/2022

ABSTRACT

The study of seismic stress distribution in subduction zones is done from two viewpoints: vector quantity study (purpose of the present study) and numerical quantity, which are important topics in seismology. The structural zone of the Makran, with the accretionary wedge as its main structure, is a kind of incremental wedge located in the hanging wall of a shallow subduction zone. In this study, earthquakes from the Harvard University Seismic Catalog (GCMT) with magnitudes equal to or greater than 5 were used. In the simultaneous inverse solving algorithm, several earthquakes were used and the stress field for different zones was calculated by the inversion method. Results of stress field analysis in the Makran zone, show heterogeneous stress fields throughout the region. Makran zone was divided into nine separate units based on structural morphology and seismic clusters. The inversion solution was performed simultaneously with several earthquakes in Michel's inverse solution algorithm, and the seismic stress field was calculated for each zone by the inversion method separately for depths less than and more than 20 km. The results of the analysis of the stress field in the Makran region show the heterogeneous spatial distribution of stress (horizontal and depth) throughout the region. The obtained stress field was compared with extended faults in each zone and active fault groups were determined. The seismic activity of the Makr an zone and its border with the adjacent tectonic zones is concentrated in several areas, which is probably due to the complex behavior of fault intersections and the interaction between fault systems. Seismic activity is concentrated in the eastern and western borders of Makran and the place where the compressive mechanism of faults (in the fold and thrust area of Makran) is converted to strike-slip regime. Another group of earthquakes occurred at the intersection of fault systems in the center of Makran and between Jazmurian depression and Moshbal, which shows the complexity of the structure at the intersection of the Sistan suture with the Makran thrust system.

Keywords:
Makran zone; Seismicity; Stress inversion; Seismic stress distribution

1. Introduction

The Makran area, with a length of about 900 km, is located in the southeast of Iran and the southwest of Pakistan as a part of the Alpine-Himalayan seismic belt (Figure 1). The seismicity of Makran is relatively low compared to other subduction zones [1]. The Makran area continues to the Las Bella axis on the eastern border after passing through Baluchistan, Pakistan. Along the axis of Las Bella, there are the main left-lateral Chaman, Ghazaband and Ornach Nal left-lateral faults, representing a transition zone between the Makran subduction zone and the Indo-Eurasian collision

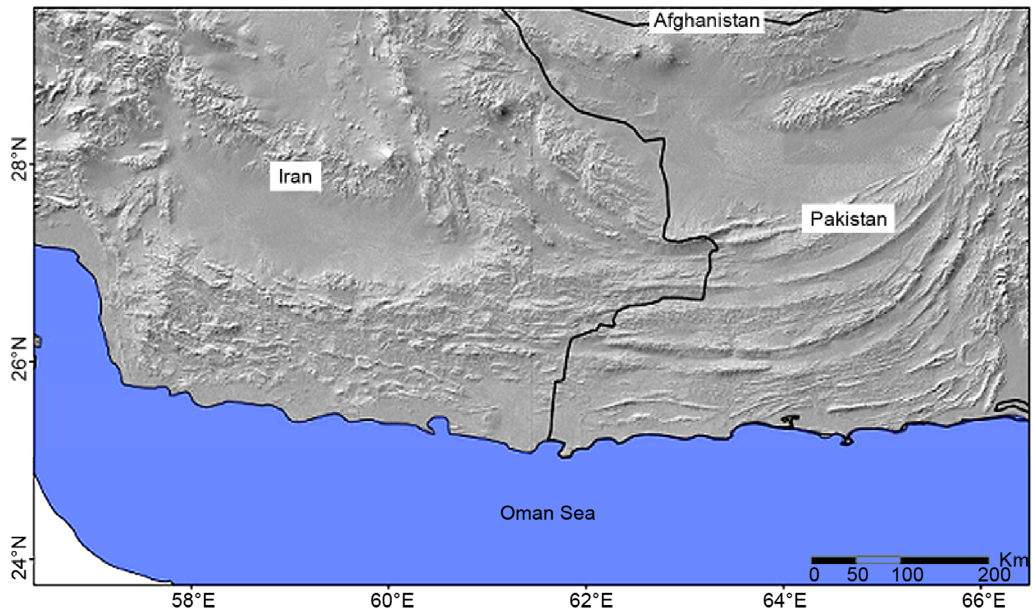

Figure 1. The Geographic location of the study area.

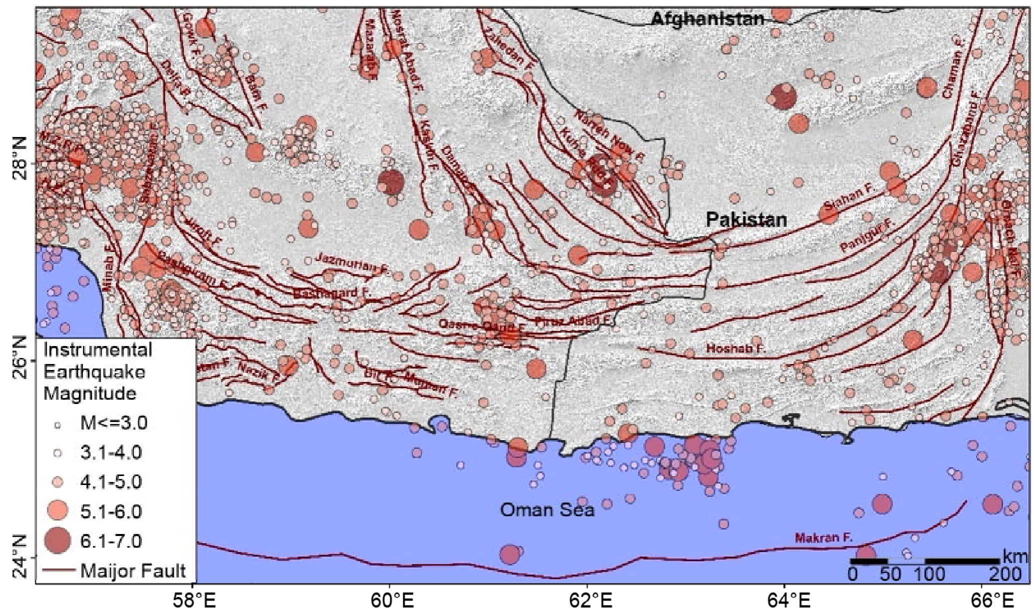

Figure 2. The location of the main faults and the distribution of instrumental earthquakes taken from the earthquake catalog (1964-2017) in the Makran zone.

zone. The Chaman fault is active in Pakistan and Afghanistan with an 850-km length. This transform system is a left-lateral strike-slip fault and forms the boundary between the Eurasian and Indo-Australian plates. Its slip rate equals the relative displacement between the above two blocks and more than 10 mm per year. This area, in addition to the strike-slip displacement component has a compressive component as a result of the collision of the Indian plate with Eurasia and forms a transpression plate boundary. This fault system starts from the south from the triple junction of the Arabian, Eurasian and Indo-Australian plates across Pakistan. Moreover, in Pakistan's Baluchistan, it extends to the north along the northeast direction to the interior of Afghanistan and joins the Pamir system.

The Makran zone on the western border is separated from the Zagros collision zone by the Zandan-Minab-Palami fault system. This system is the border between the two convergent continental plates of Zagros and the active oceanic crust of the Oman Sea (Figure 2). The structure of accretionary wedges of Makran has been bordered by steep reverse faults. The operation of this structure has caused fault sheets to be driven from the hinterland in the North-East to the foreland in the South-West [2-3]. Makran subduction rate increases slightly from west to east [3]. This rising rate is not the same throughout the length of Makran (Western and Eastern Makran).

Normand et al. [4] obtained the uplift rate between 0.05 and 1.2 mm per year in the east-west direction. The geodetic observation data has shown the convergence rate between the Makran coast (Chabahar GPS station) and the Eurasia is about 8 mm per year, equal to the rate of shortening within the accretionary wedge. The continuity of convergence and subduction of the oceanic crust of Oman is confirmed by the continuous rise of the coastal terraces in the present time along with the advance of the coastline towards the sea [5]. These pieces of evidence indicate the functioning of the subsurface tectonics and the activity of hidden thrusts along and above the active detachment thrust surfaces (Detachment fault-Decollement) and the dominant right-lateral strike-slip deformation in the West Makran (in Iran) around the Minab fault system was the cause of seismic ruptures in this part of Makran [6].

The main purpose of this research is to determine the seismic stress tensors in the Makran region using the earthquakes' mechanisms. Since the stress tensor cannot be accurately determined using the focal mechanism of only one earthquake, the simultaneous inverse solution algorithm of several earthquakes has been used.

2. Tectonic and Seismicity

The Makran subduction zone, as an Arc-Trench system, has the most extended length of its kind [7]. The Makran accretionary wedge has been created as a wedge with a low slope due to the active subduction of the oceanic lithosphere of the Oman Sea under the Lut and Afghan continental blocks, since the Cretaceous [7-12]. The distance between the arc and trench reaches 500 km. Ocean trenches develop in subduction zones with a depth of about 2-4 km on the ocean floor [13-15].

The active subduction of Makran is associated with the folding, shortening and regression of the coastline. The deformation in the Makran region with two main horizons of Middle Miocene shales and Upper Oligocene shales as detachment surfaces is of thin skin type of tectonics. On the other hand, seismic data in the marine part indicate the presence of an active detachment thrust at a depth of 10-15 km under the inner Makran [16]. The epicenter of the earthquakes and the seismic data in the marine part show that the subduction of the oceanic lithosphere is done with a slope of less than 3 degrees towards the north. The depth of this plate under Jazmurian depressions reaches 30 km [1, 17].

Based on the observations of coastal geology and seismology, in some studies, the subduction zone has been considered to include two different areas that are located in the east and west of the Sistan suture, a structure that is the continuation of the Sonia fault system located in the sea [17-19]. Burg [20] and Dolati and Burg [16] divided Makran into four separate units that are separated by Beshagard, Qasr Ghand and Chah Khan Thrust fault zones (Figure 2).

Mokhtari et al. [21], in the analysis of tomography data, obtained a gentle slope of 3-5 degrees in the distance of 50 to 150 km north of the Coast of the Oman Sea for the subduction plate. The results show that the subsurface part of North Makran (at a depth of 20 km) has medium or even higher crustal velocities. This anomaly indicates the mixing of mafic ophiolitic materials and metamorphic rocks, which has a high-velocity anomaly. In the southern parts, a sudden change of anomaly has taken place in the parts with lower seismic speed. This unit corresponds to the Beshagard fault, which is the boundary between the northern unit of Makran and the internal unit.

Despite the different seismicity, the main structural elements inside the accretionary wedge in the east and west of Makran have a dip towards the north [14, 22-24]. The basic structures of the region include folds and faults. Makran folds have an approximate east-west trend, which is in harmony with the direction of maximum shortening and maximum stress in the northeast direction. Shortening is mainly associated with thrusting so the boundary of many stratigraphic units is thrust type. Often, the anticlines are narrow and reversed and are seen along with asymmetric synclines with an east-west axial direction. At each stage of convergence, a slice of the sedimentary wedge is added to the north continental block during the over-thrusting phenomenon. Therefore, from south to north, an increase in age, uplift rate, height, the density of active faults and folds, as well as deformations and metamorphism, can be seen in flysches [11].

In the Makran area, the mechanism of continental crust earthquakes are of all three types strike-slip, thrust, and normal (mainly with a depth of less than 50 km) (Figure 3). Due to the north-south compressive tectonic regime, there are three types of fracture and faulting systems in Makran: 1- Reverse faults with east-west direction, the main large faults of the region are formed by the reverse mechanism with a dip towards the north. These faults seem to be caused by the continued activity of the imbricate faults in the accretionary wedges. The Beshagard fault system and the Qasr Khand fault can be mentioned as examples of this type of faults. Makran strike-slip faults are mostly left-lateral and the rake angle of their slikenlines is less than 20 degrees. The strike-slip faults along the NW-SE direction are generally right-lateral, and the rake angle of their slikenlines is less than 20 degrees. These faults have acted as conjugate faults and cut the east-west trend of the structures and prove a convergence towards the north inside the accretionary wedge.

King et al. [25] presented that the depth of normal faults is up to 20 km. Minor normal faults extend in the east-west direction in the two coastal

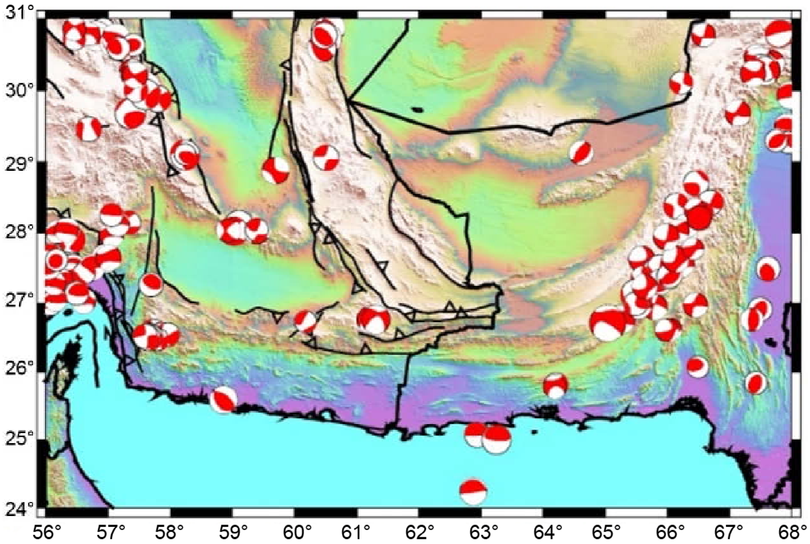

(a) Earthquakes at a Depth of Less than 20 km

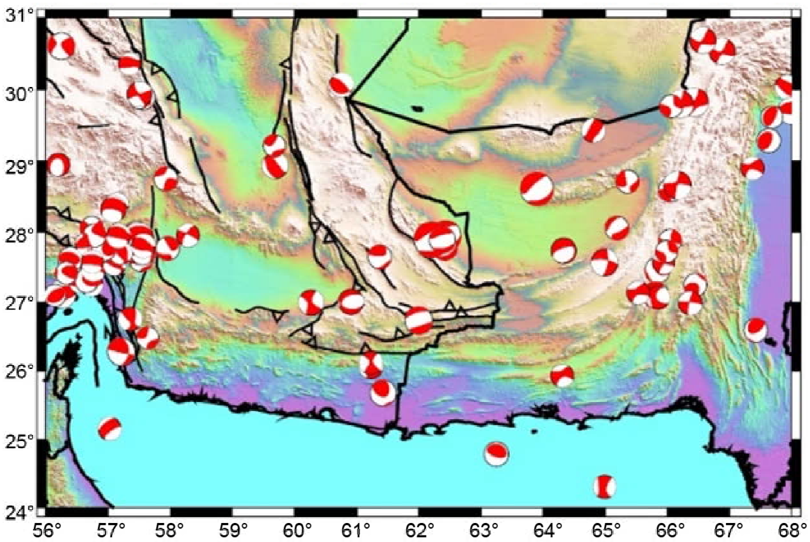

(b) Earthquakes at a Depth of More than 20 km.

Figure 3. The focal mechanism of earthquakes in the Makran Zone based on Appendix 1 (GCMT).

areas and the edges of the Jazmurian depressions. The main dip of the coastal normal faults with Quaternary age is towards the south and the dip of most of the normal faults of the Jazmurian margin is towards the north. The linearity of the northern edge of the marine terraces and the rising of the Makran coast are the result of the action of these faults, and the vertical movements of these faults have caused the marine terraces to be formed at different levels [26].

Almost all earthquakes in the western part of Makran occur within the subducting plate and at medium depths, and they often have a normal mechanism. The lack of plate boundary earthquakes in West Makran can indicate aseismic subduction or the current locking of the plate boundary [8, 17] and the occurrence of earthquakes with a very long return period. The finite element adhesive elastic model results show that high friction coefficient and low convergence speed can slow down the process of shear stress accumulation and affect the seismic behavior in the forearc environment. This factor can justify the low seismic activity [27]. The presence of negative and strong gravity anomalies and the parallel topography of the trench in the west of Makran indicate a strong coupling in this region [27]. Due to the high friction coefficient at the plane boundary, the abducted bedrock is pulled down with the subducted bedrock. Studies [28-30] show that large earthquakes often occur in areas with strong negative gravity anomalies. Based on this, areas in the fore-arc with TPTA (Trench Paralle Topography Anomaly) less than 750 meters below the open sea level and TPGA (Trench Parallel Gravity Anomaly) less than -40 milligal are prone to large earthquakes. The amount of TPTA and TPGA in the west of Makran is strongly negative compared to the east. According to the research of Pacheco et al. [31], the presence of large earthquakes (such as the 1945 earthquake) in the east of Makran is consistent with more positive values of TPTA and TPGA in the forearc regions.

Shallow seismic activities start from the coast and continue inland up to a distance of about 70 kilometers from the coast. The earthquakes become deeper due to the beginning of the bending slab. The depth of the hypocenters continues to the south of the volcanic arc and reaches 80 kilometers. At the bottom of this depth, only a few earthquakes between 80 and 100 km have been recorded [2, 32]. On the other hand, the large earthquakes located in the north of Makran and Jazmurian and Mashkel depressions have medium depth [17].

Normal faults limit the southern border of these depressions with a dip to the north [20]. These earthquakes are generally classified as intraslab earthquakes. The study of seismicity, solving focal mechanisms and geological evidence in the Makran area shows that normal faulting causes moderate-depth earthquakes. Normal faults parallel to thrust faults with seismic activity in this area have an approximately parallel direction. These faults are mainly located in the coastal and northern parts of the accretionary wedges in the hanging wall of the subduction zone.

Some consider normal earthquakes related to the intersection of the normal faults south of the Jazmurian and Mashkel depressions with the wedges [6]. Normal faults of the same age and parallel to the thrusts are formed independently of the thickness of the crust, height and scale [33-34].

The mechanism of smaller earthquakes is compatible with the Strike of Faults and their epicenter is placed on the faults [35-36]. Lin et al. [37], based on the distribution of seismic coupling in abduction of the East Makran fault from 2003 to 2010, concluded that seismic coupling occurred in the central part of the eastern Makran at the site of the 1945 earthquake. The change of the axis of maximum seismic stress based on previous studies in Makran region is shown in Figure (4). According to the previous results (38-39), the maximum stress axis rotates from the west to the east of Makran (38-39). In the western part of Makran, the maximum horizontal stress orientation was 17.6±4, parallel to Zagros, and showed the effect of the continent-continent collision between Arabia and Eurasia plates. In Central Makran, this direction showed a clockwise rotation and became 38.2±3. In the eastern part, which is under the influence of the continent-continent collision between Indian and Eurasian plates, the direction was 157.0±4.

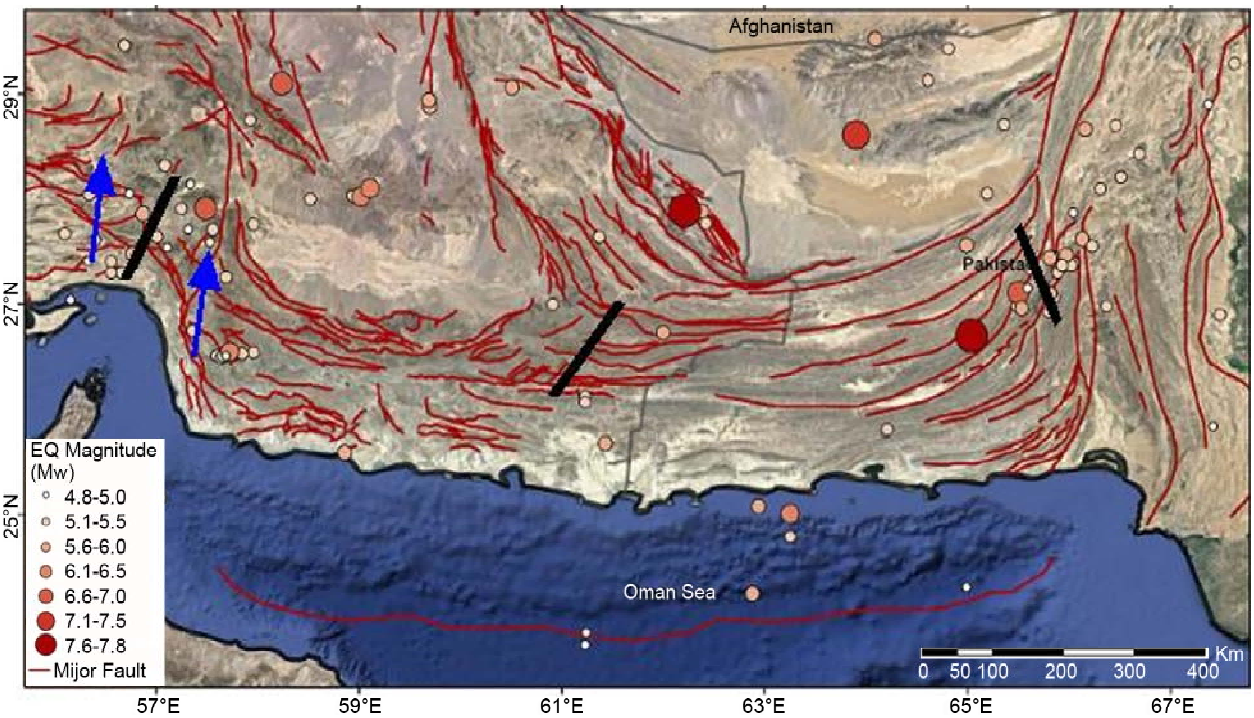

Figure 4. Seismotectonic map of the Makran structural zone. Black bars are the maximum stress direction from earthquake focal mechanisms [38]. These directions showed a variation acceptable according to the region's tectonic state and previous studies in the area. Blue arrows represent the direction of the maximum compressive stress obtained by Rostam et al. [39]. The earthquakes are obtained from the IIEES earthquake catalog.

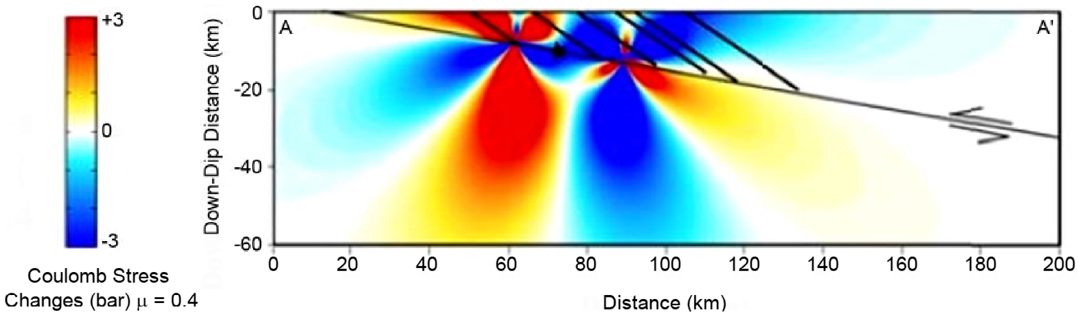

Figure 5. Coulomb stress changes due to the hypothetical earthquake (Mw=7.2) assumed at a depth of 10 km for µ'=0.4 [40].

Mehr et al. [40] calculated Coulomb stress changes along the splay faults following a hypothetical earthquake (Mw = 7.2) on the mega-thrust (Figure 5). The amount of slip that transfers from the plate boundary onto the splay faults during a large subduction earthquake and the pattern of slip partitioning between them are calculated. The results show that the slip on mega-thrust increases stresses in some surrounding areas. Some splay faults are located in these areas that can be loaded in shallow depth and are likely the sources of aftershocks.

According to the kinematic studies of the faults in eastern Iran [41], at 61 degrees to the σ_1-axis in the east of Lut block, it has experienced 65 degrees counterclockwise rotation in less than 10 million years. The azimuth of the maximum stress axis was 90 degrees in the Miocene, 60 degrees in the late Pliocene, and 25 degrees in the Plioquaternary. Therefore, at present, in the northern parts of the Sistan suture (at approximately 32 degrees latitude), there is a strong pressure field that is in agreement with the convergence direction of the Iranian and Arabian plates and the effective stress transfer from the Zagros collision zone to Sistan and the shortening in the direction of the Sistan suture. Nevertheless, the change of the stress field in the southern splay faults of the Sistan suture fault can be related to the subducting slab boundary earthquakes.

This area has been subjected to several studies, including [42] the depth and geometry of the fault in Qeshm Island, located in the western part of the transitional border. The results of the analysis of radar interferometric data and tele-seismic data and local network on three major Qeshm earthquakes (November 2005, June 2006 and September 2008), the relationship between buried thrust faults and surface fold structures was determined. Seismic faults in large earthquakes are generally perpendicular to the axial plane of the folded Zagros. Furthermore, probably the structure of deep faults and surface folds are separated along the weak marl or evaporite layers in the middle part of the sedimentary cover [43].

On the western edge of the Lut structural block, the Zandan-Minab-Palami fault system consists of several faults corresponding to the transpressional tectonic regime. The Zandan-Minab-Palami fault system consists of several faults corresponding to the transpressional tectonic regime. The surface manifestation of this deep fault system is the north-south right-lateral strike-slip Jiroft-Sabzevaran fault system, which is composed of smaller faults that together form a strike-slip fault system (Wrench fault) on the lithospheric scale. The Jiroft-Sabzvaran fault system connects to the Gowk-Nayband fault system (western border of Lut block) towards the north.

3. Data

In this study, more than 150 earthquakes taken from the Harvard Seismic Catalog (CMT) were included in the calculations. All earthquakes with a magnitude equal to or greater than 5 in Makran and adjacent areas are shown in Appendix (1). In the Harvard seismology network, the recorded seismic data is analyzed based on the algorithm provided by Dezinovsky [44]. In this center, the waveform data can be used not only to extract the earthquake source mechanism but also to determine the coordinates of the subsurface center (stress saturation density center) at a certain frequency. Thus, two classic problems of seismology are combined in a single method. Considering the estimation of origin time, central coordinate and depth, the initial moment tensor is described in detail by Dziewonski et al. [44]. The upper limit of the magnitude of earthquakes that can be processed using this particular approach appears to be 8.0 and the lower limit is approximately 5, but this can be extended by extending the passband to periods shorter than 45 seconds [44].

4. Method

Some researchers study stress in the crust and determined tectonic stress from focal mechanisms of earthquakes in the past [45]. The most ordinary used algorithm have been expanded by [46-48] with changing and added proposed by [45, 49-51] and others. These inversion algorithm usually assume that (1) tectonic stress is uniform (homogeneous) in the region, (2) earthquakes occur on pre-existing faults with varying orientations and (3) the slip vector points in the direction of shear stress on the fault (the so-called Wallace-Bott hypothesis) [52-53]. If the above foresaid assumptions are content, the stress inversion methods are capable of determining four parameters of the stress tensor: three angles defining the directions of principal stresses, σ_1, σ_2 and σ_3, and shape ratio R [47]:

$$R = \frac{\sigma_2 - \sigma_1}{\sigma_3 - \sigma_1} \tag{1}$$

The methods are weakly to meliorate the residual two parameters of the stress tensor. Therefore, the trace of the stress tensor is usually assumed to be zero [46]:

$$Tr(\boldsymbol{\tau}) = \sigma_1 + \sigma_2 + \sigma_3 = 0 \tag{2}$$

and the stress tensor is normalized.

The stress inversion method developed by [46] employs expressions for normal and shear tractions on a fault σ_n and τ:

$$\sigma_n = T_i n_i = \tau_{ij} n_i n_j \tag{3}$$

$$\begin{aligned} \tau N_i &= T_i - \sigma_n n_i = \\ \tau_i n_j - \tau_{jk} n_j n_k n_i &= \tau_{kj} n_j \left(\delta_{ik} - n_i n_k\right) \end{aligned} \tag{4}$$

where δ_{ik} is the Kronecker delta, T is the traction along the fault, n is the fault normal and N is the unit direction vector of shear stress along the fault. Subsequently, Equation (4) is modified to read:

$$\tau_{kj} n_j \left(\delta_{ik} - n_i n_k\right) = \tau N_i \tag{5}$$

In order to be able to evaluate the right-hand side of Equation (4), Michael [46] applied the Wallace-Bott assumption and identified the direction of shear stress N with the slip direction s of shear motion along the fault. He further assumed that shear stress τ on activated faults has the same value for all studied earthquakes. Since the method cannot determine absolute stress values, τ is normalized to be 1 in Equation (5). Subsequently, Equation (5) is expressed in matrix form:

$$At = s \tag{6}$$

where t is the vector of stress components,

$$t = \left[\tau_{11}\tau_{12}\tau_{13}\tau_{22}\tau_{23}\right]^T \tag{7}$$

A is a 3×5 matrix calculated from fault normal **n**,

$$\begin{vmatrix} n_1(n_2^2 + 2n_2^2) & n_2(1-2n_1^2) & n_3(1-2n_1^2) & \ldots \\ n_1(-n_2^2 + n_3^2) & -2n_1n_2n_3 & & \\ n_2(-n_1^2 + 2n_3^2) & n_1(1-2n_2^2) & -2n_1n_2n_3 & \ldots \\ n_2(n_1^2 + n_3^2) & n_3(1-2n_2^2) & & \\ n_3(-2n_1^2 + n_2^2) & -2n_1n_2n_3 & n_1(1-2n_3^2) & \ldots \\ n_3(-n_1^2 - 2n_2^2) & n_2(1-2n_3^2) & & \end{vmatrix} \tag{8}$$

and s is the unit direction of the slip vector.

Extending Equation (8) for focal mechanisms of K earthquakes with known fault normals n and slip directions s, we obtain a system of $3K$ linear equations for six unknown components of the stress tensor. Finally, we include Equation (2) and solve the system using the generalized linear inversion in the L2-norm [54].

As follows from the above Equation, the basic drawback of Michael's method is the necessity to know the orientations of the faults [55]. If Michael's method is used with incorrect orientations of the fault planes, the accuracy of the retrieved stress tensor is decreased. Michael [55] performed a series of numerical tests and found that, in particular, the shape ratio can be distorted. On the other hand, the method is relatively fast and can be run repeatedly. Therefore, the confidence regions of the solution can be determined using a standard bootstrap method [55]. If the orientation of fault planes in focal mechanisms is unknown, each nodal plane has a 50 percent probability of being chosen as the fault during the bootstrap re-sampling.

4.1. Differential Stress

Considering the seismicity analysis by Spada et al. [56] for magnitudes greater than 2.5 in various continental domains and for different styles of deformation, Scholz [57] defined a relationship between b-value and differential stress (σ_1-σ_3) as follows:

$$b = 1.23 \pm 0.06 - \left(0.0012 \pm 0.0003\right)\left(n_1 - n_3\right) \tag{9}$$

where (σ_1-σ_3) is in mega Pascal. The author shows that this relationship explains that both the seismicity distribution with depth and the type of focal mechanism are related to the b-value.

This equation outlines the negative correlation between the two variables, i.e. a high b-value corresponds to a low differential stress and a low b-value to a high differential stress.

It is worthy to note that, in Equation (9), if b-value is greater than 1.23, (σ_1-σ_3) is negative, which is physically unusual. It must be kept in mind that Equation (9) results from the linear fit of a large number of scattered data where some b-values exceed 1.23. It is thus a simplified model. This marks the limits of the use of this relation as values of b greater than 1.23 are not rare.

5. Results

Makran area is divided into nine separate units based on morphological and structural units, earthquake clusters and geological studies. The stress field for each zone is calculated by the Michel inversion method [46] defined in Zmap software. The results of stress field analysis in the Makran zone show non-uniform stress fields throughout this area (Figures 6 to 13 and Tables 1 and 2).

Zone No. 1 is located on the Sistan suture zone and at the intersection of the north-northwest-south-southeast strike-slip faults of Iran's eastern border with the Makran fold and thrust zone. The change in the direction of the faults can be considered as splay faults of the north-south faults in the east of Iran. The present study shows the

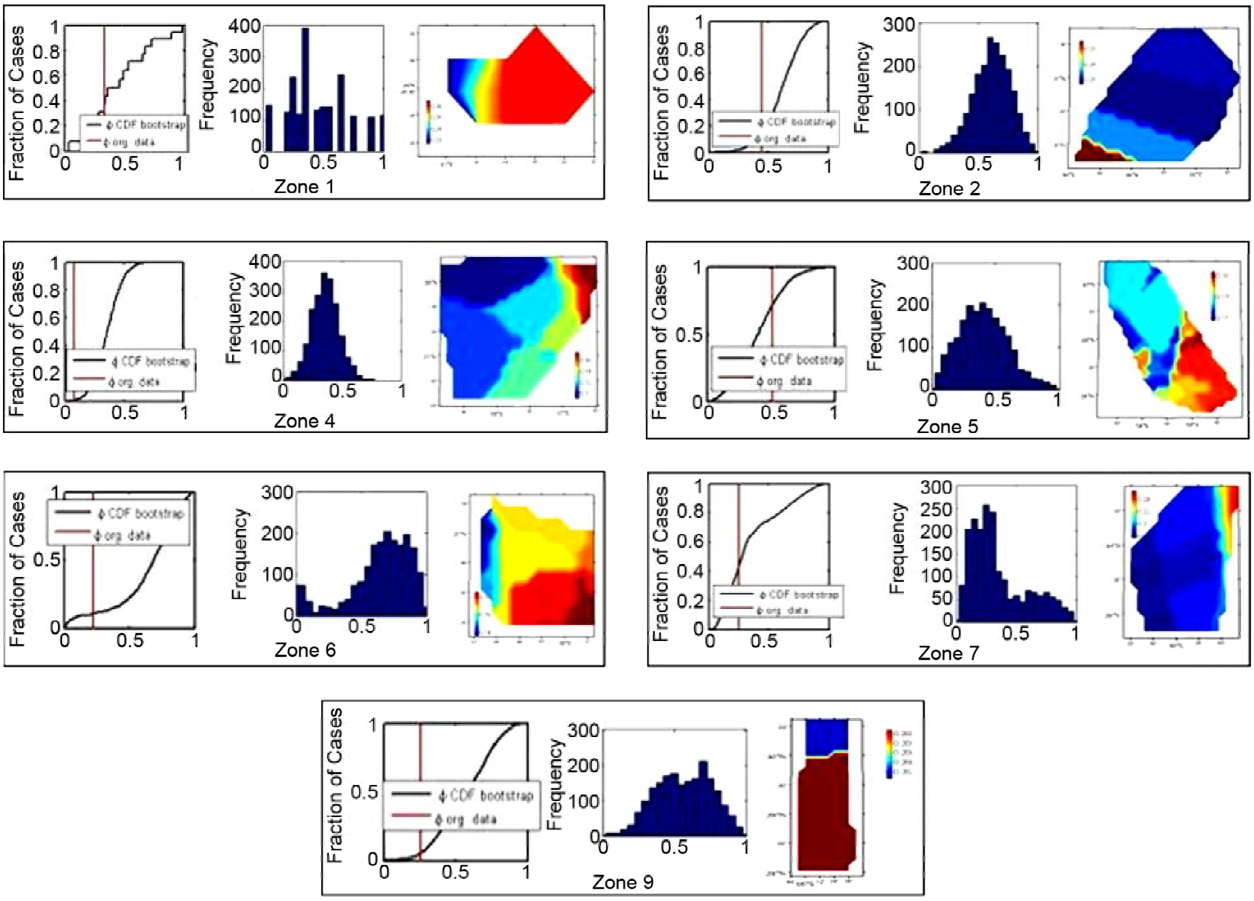

Depth < 20 km

Figure 6. From left to right (a) the ratio of changes in stress difference (R), (b) the ratio of histogram shape (R). (c) the calculated error rate related to the maximum stress (σ_1) For seismic zones (depth < 20km).

Table 1. It shows the extracted values from the inverse solution for earthquake source with depth < 20 km.

Number of Blocks	The Direction and Plunge of Stress (S_1^0) in Stereonet		The Direction and Plunge of Stress (S_2^0) in Stereonet		The Direction and Plunge of Stress (S_3^0) in Stereonet		phi	Variance	Mechanism
1	9.1	34.8	107.8	12.4	-145.5	52.4	0.34±0.248	2e-030	Thrust
2	151.4	6.2	-91.1	76.7	60.1	11.6	0.440±0.1560	0.047	Strike- Slip
3	-	-	-	-	-	-	-	-	-
4	174.4	0.6	-95.2	19.5	-82.9	70.4	0.076±.1107	0.059	Thrust
5	47.8	18	-99.8	69	141.2	10.5	0.51±0.18978	0.11	Strike- Slip
6	30.4	4.8	128.5	59	-62.5	30.5	0.22±0.25194	0.00049	Strike- Slip
7	--13.3	0.8	139.4	8.8	-35.1	81.2	0.25±0.23639	0.014	Thrust
8	-	-	-	-	-	-	-	-	-
9	145.4	4	43.9	70.6	-123.1	18.9	0.26±0.19248	0.014	Strike- Slip

seismic stress field at two depths of less than 20 km and more than 20 km separately. The results of the stress inversion can be seen in Figures (8) and (9) in terms of the azimuth and plunge of the maximum (σ_1), medium stress (σ_2) and minimum (σ_3) principal stress axes (where $\sigma_1 > \sigma_2 > \sigma_3$). Earthquakes at a depth of less than 20 km, have generally occurred in the compressive oblique stress field with the right lateral strike slip component. The trend of the maximum horizontal stress axis was 9 degrees with a plunge angle of 35 degrees, a trend of 108 degrees and a plunge of 12 degrees, and a trend of -145 degrees and a plunge of 52 degrees, respectively, for the average and minimum main horizontal stresses.

Our stress inversion results for zone no 1 (depth < 20 km) indicate that the σ_1 axes are orientated N_S, with plunge equal to 34.8°, suggesting a compressional tectonic. This is confirmed by the almost vertical 63 axes. The results indicate that the

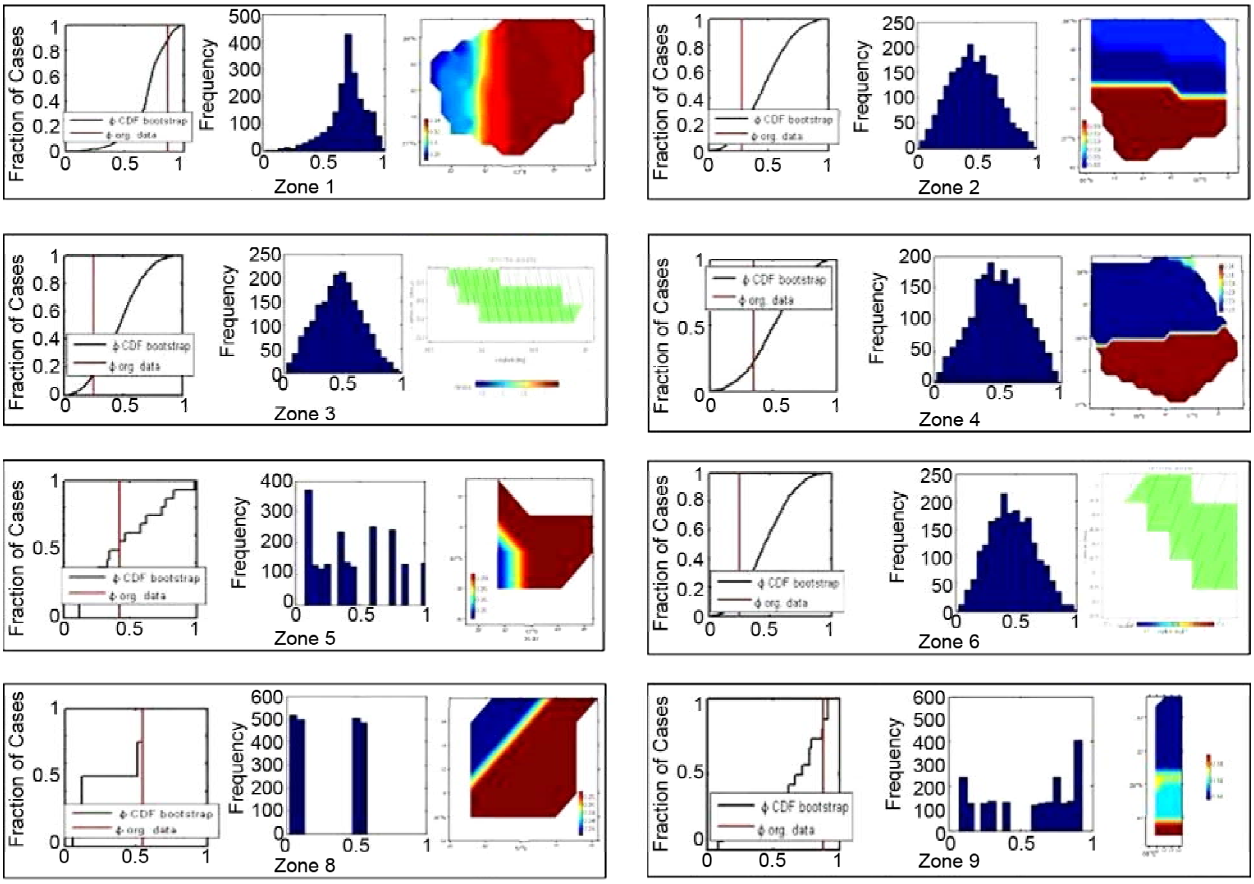

Depth > 20 km

Figure 7. From left to right (a) the ratio of changes in stress difference (R), (b) the ratio of histogram shape (R). (c) the calculated error rate related to the maximum stress (σ_1) For seismic zones (depth > 20km).

Table 2. It shows the extracted values from the inverse solution for earthquake source with depth > 20 km.

Number of Blocks	The Direction of Stress (S_1^0) in Stereonet		The Direction of Stress (S_2^0) in Stereonet		The Direction of Stress (S_3^0) in Stereonet		phi	Variance	Mechanism
1	-111.9	6.1	122.8	79.4	-21	8.5	0.87±0.15594	0.014	Strike-Slip
2	-165	4.4	104.3	7.3	-44.2	81.4	0.28±0.19522	0.32	Thrust
3	-170.3	1.8	-80.1	8.9	87.9	80.8	0.25±0.1899	0.32	Thrust
4	6.1	2.8	-84.5	12.2	108.7	77.4	0.35±0.20274	0.19	Thrust
5	24.4	18.4	141.9	54.3	-76.3	29.3	0.42±0.27851	1e-031	Strike-Slip
6	-170.3	1.8	-80.1	8.9	87.9	80.8	0.25±0.1888	0.32	Thrust
7	-43.4	7.5	47.3	6.1	176.2	80.2	0.16±0.193	0.012	Reverse
8	151.8	37.3	14.2	44.1	-99.5	22.6	0.55±0.22215	1.3e-031	Unknow
9	-33.8	4	57.1	12.5	-141.2	76.8	0.88±0.29646	4.7e-030	Thrust

seismic stress field at a depth of more than 20 km, the σ_1 axes are orientated E-W, with plunge equal to 6.1°, suggesting a compressional tectonic.

Zone 7 is located in the east of the Lut block and in the north of zone 1. This area includes Sistan suture (28-29 degrees north latitude) between the area studied by Jentze et al. [41] and zone 1.

Our stress inversion results for zone no7 (depth < 20 km) indicate that the ?1 axes are orientated NE_SW, with plunge equal to 0.8°, suggesting a compressional to transpressional tectonic. This is confirmed by the almost vertical 63 axes. No earthquake with a magnitude of more than 5 at a depth of more than 20 km has been recorded in this zone.

The zone No. 4 is located at the transitional boundary of the Zagros and Makran Subduction Zones and is at the intersection of the Oman structural line, the Zendan-Minab fault zone and the Faults of Zagros Zone. The seismic stress field

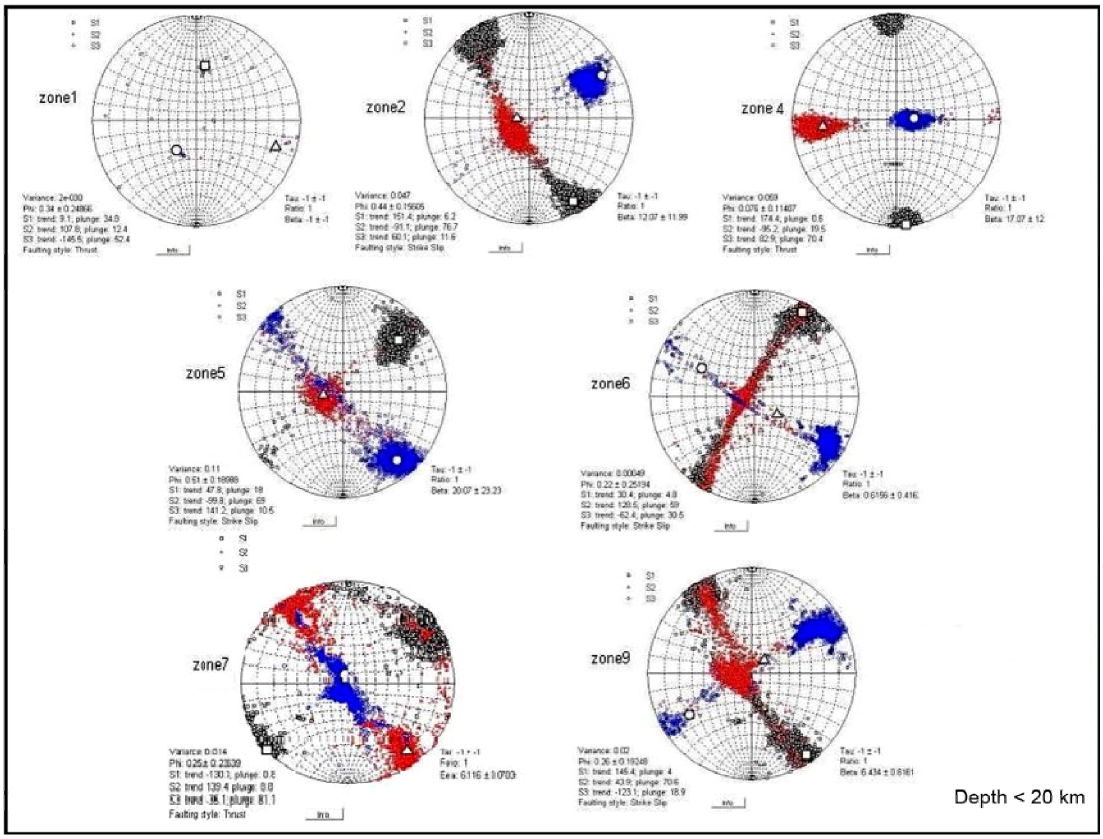

Figure 8. It shows the results of seismic stress inversion in the three-dimensional plane of the stereonet (depth < 20 km). The white square shows the maximum stress level (σ_1), the white triangle shows the average stress level (σ_2). The white circle shows the minimum stress level (σ_3).

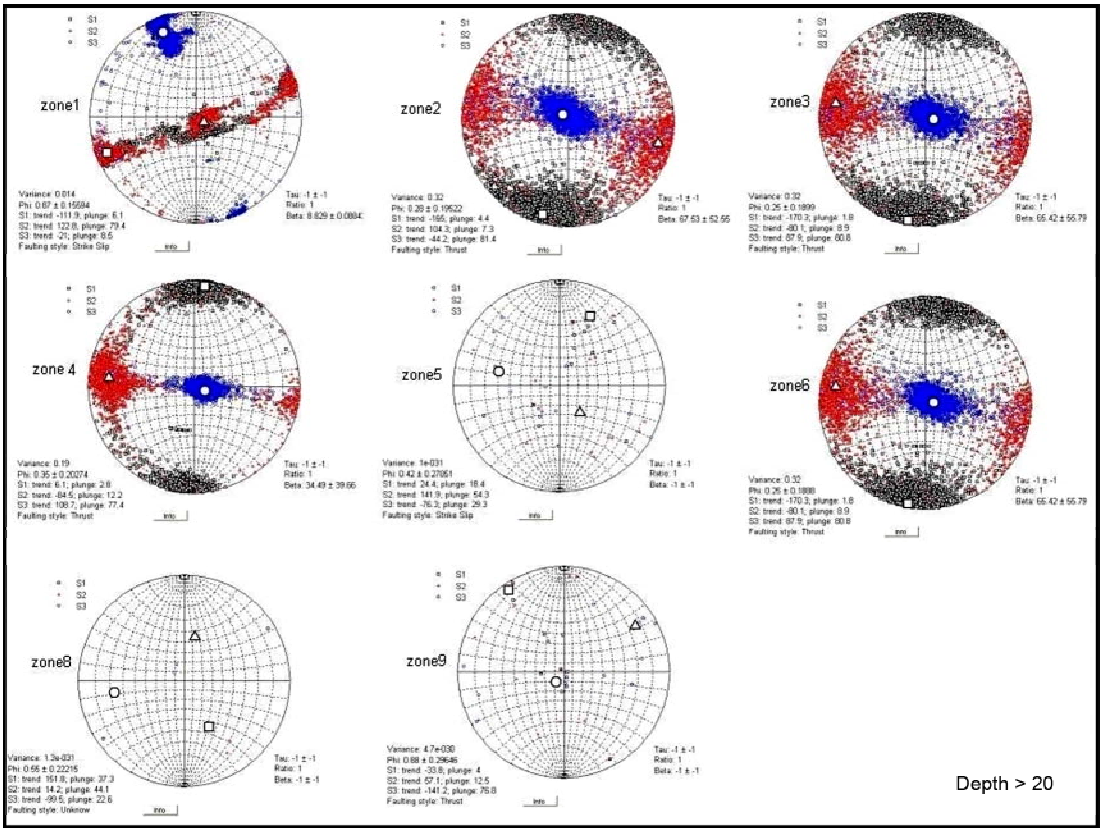

Figure 9. It shows the results of seismic stress inversion in the three-dimensional plane of the stereonet (depth > 20 km). The white square shows the maximum stress level (σ_1), the white triangle shows the average stress level (σ_2). The white circle shows the minimum stress level (σ_3).

in this zone has a small rotation with depth changes and according to the fault strike direction located in the Zagros zone is a compressive field with a small strike-slip component. The Stress Field obtained in Depth < 20 km is effective on compressive structure and thrust faults and can be attributed to their activity. The stress field in depth > 20 km is probably affects the left lateral faults of structural zone of Oman [58]. The interaction between the Oman structural zone and the Zagros folded zone faults explains the bending along the Zagros thrust faults on the eastern edge of the Zagros.

The stress field calculated in area No. 5, located in the western part of the Lut block, is the right-lateral strike-slip fault zone. The main faults in this area are compressive and right-lateral strike-slip faults on Bam, Delfa Gowk, Sardoyeh, oblique-slip faults, Rain (compressive and right-lateral strike-slip fault), Shahdad and Khardum faults, Mahan faults, Jabal Barez and Chah Mazraeh with an unknown mechanism. The general direction in this area is north-northwest-south-southeast. The results of our study shows that the seismic stress in the west of the Lut block (zone no. 5) at a depth of less than 20 km is oblique slip and Compressive. The stress field undergoes slight rotation with increasing depth.

Zone 6 is located in the right-lateral tectonic regime with splay faults in the West Makran. Based on the calculated stress field, the effective tectonic structures of this part are probably buried and have the northeastern-southwestern strike and effect similar to the dominant deformation of zone no. 5 On the west side of Lut block [59]. Figures (8) and (9) indicate the variation in plunge of the σ_3 axes at depth > 20 km and depth < 20 km Earthquakes at a depth of less than 20 km, have generally occurred in the transpression tectonic. The trend of the maximum horizontal stress axis is 30.4 degrees with a plunge angle of 4.8 degrees. As the depth increases, the compressive component of the seismic stress field increases.

Our stress inversion results for zone no 1 (depth < 20 km) indicate that the σ_1 axes are orientated N_S, with plunge equal to 34.8°, suggesting a transpression tectonic. This is confirmed by the almost vertical 63 axes. The results indicate that the seismic stress field at a depth of more than 20 km, the σ_2 axes is vertical, suggesting a transpression tectonic.

Zone 7 is located in the east of the Lut block. This area includes Sistan suture (28-29 degrees north latitude) between the area studied by Jentzer et al. [41] and zone 1. Our stress inversion results (depth < 20 km) indicate that the σ_3 axes is vertical, suggesting a compressional to transpressional tectonic. This is confirmed by the almost vertical σ_3 axes. No earthquake with a magnitude of more than 5 at a depth of more than 20 km has been recorded in this zone.

The seismic stress field in the northern parts of Chaman and Ghazaband transform faults is dependent on the depth change. At a depth of less than 20 km, the strike-slip stress field with a partial compressive component is dominant, and with increasing depth, the seismic stress field becomes compressive. This situation is different from the western border of the Makran zone, which is probably because the eastern border of the Makran zone is more strongly affected by the Indo-Eurasian convergence forces.

The comparison of the stress fields at the southern end of the eastern border of the Makran zone in two depth ranges (less than and more than 20 km) shows that the stress field is almost constant (right-slip with a partial component of dip-slip with steep nodal surfaces) and with partial rotation. The stress field increases with depth of earthquakes. The trend and plunge of the axis of the maximum stress at a depth less than 20 km are equal to 151 degrees and almost horizontal. At depth of less than 20 km, the angles of the trend and axis of the average stress are equal to -91 and 77 degrees, respectively, which indicate the strike-slip stress field. In contrast to the seismic stress field at a depth of more than 20 km, the angles of the trend and inclination of the maximum stress axis are -165 and 4 degrees respectively, and the trend and inclination of the minimum stress axis are -44 and 81 degrees respectively, which indicate the field compressive stress.

In the east of Makran (areas no. 2, 3 and 9), the main left-lateral Ornach Nal fault, Ghazaband fault and the Bela-Chaman fault zone extend and

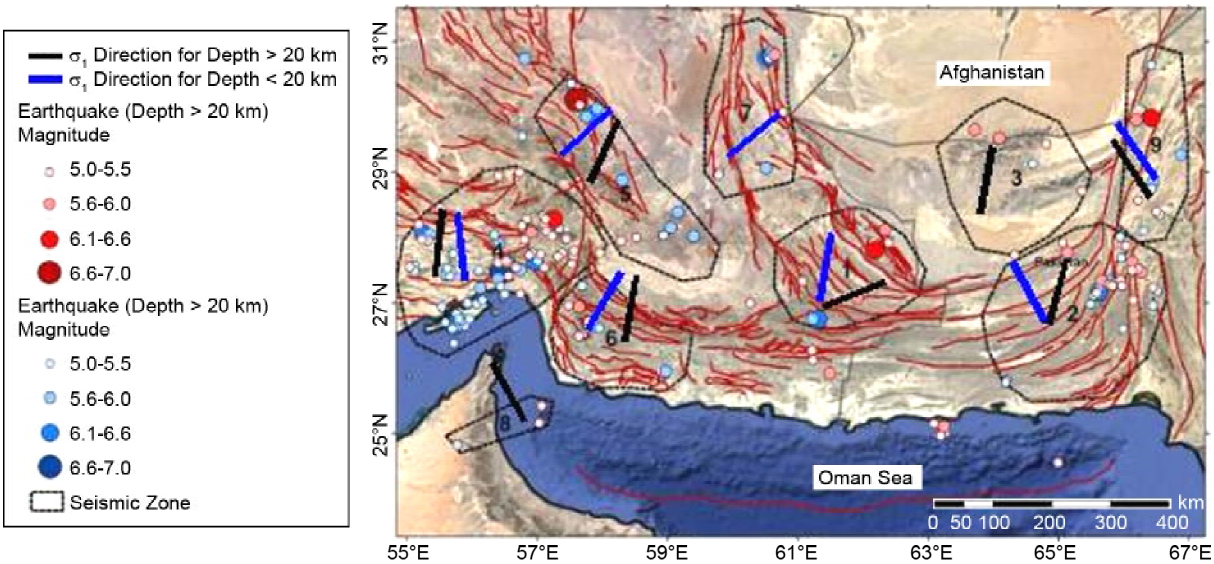

Figure 10. Distribution of selected seismic zones in the Makran area. Blue arrows represent the direction of the maximum compressive stress at depth < 20km and black arrows represent the direction of the maximum compressive stress at depth > 20km.

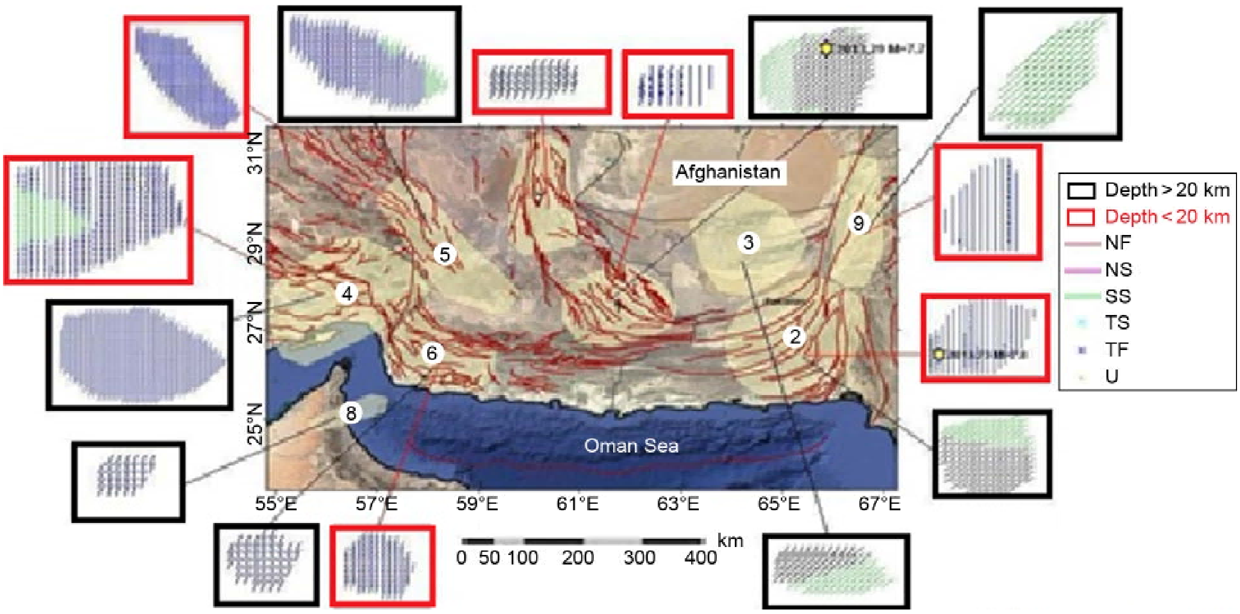

Figure 11. It shows stress tensor vectors and the type of dominant mechanisms in the studied zones.

are effective. The trend of maximum stress axis in the east of Makran zone from 35 to 60 degrees.

In these three zones, the seismic stress field at a depth of less than 20 km is strike-slip (the maximum stress is northwest-southeast striking and almost horizontal). Therefore, it causes the displacement of left lateral strike-slip on the transform faults of the eastern margin of Makran, on the other hand, it causes the compressional displacement on the ENE-WSW striking splay faults and thrusts of Makran zone. The stress field at a depth of more than 20 km is compressive in zones 2 and 3, and the maximum stress is parallel to the convergence of the plates.

Our stress inversion results for zones no 1 (depth < 20 km) indicate that the σ_1 axes are orientated N_S, with plunge equal to 34.8°, suggesting a transpression tectonic. This is confirmed by the almost vertical 63 axes. The results indicate that the seismic stress field at a depth of more than 20 km suggesting a transpression tectonic (the σ_2 axes is vertical).

Horizontal orientation of S1 (blue and black) principal stress axes and stress tensor vector for focal mechanisms of selected earthquakes ($H \leq 20$ km and H > 20 km) in Makran zone prepared in

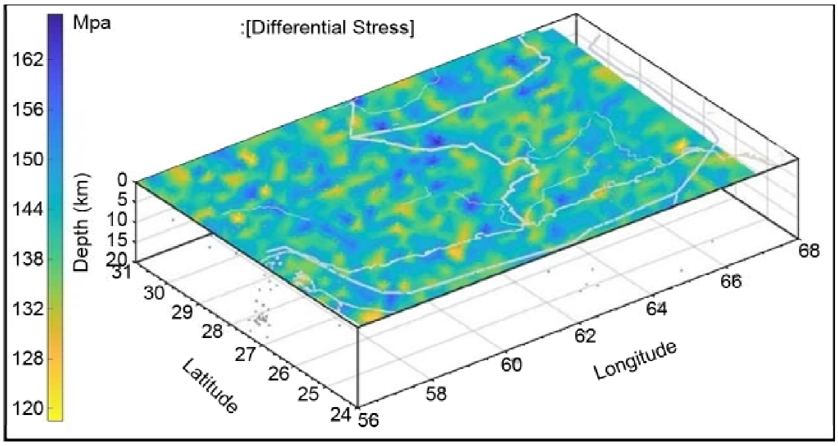

Figure 12. Contour map of differential stress field (σ_1-σ_3) for earthquake source with depth of less than 20 km in Makran region.

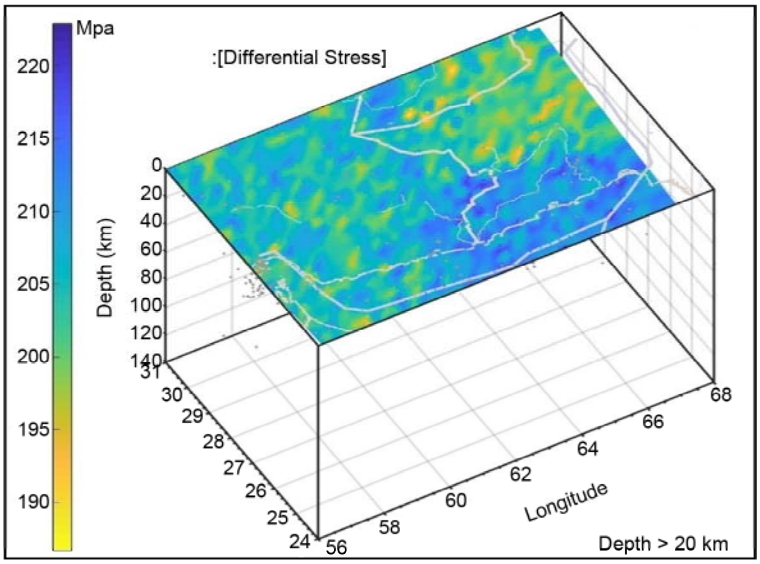

Figure 13. Contour map of differential stress field (σ_1-σ_3) for earthquakes with depth of more than 20 km in Makran region.

Figure (10) and Figure (11), respectively.

Referring to our latest study [60], the Makran zone was evaluated by considering the concepts of seismicity parameters considered in the Gutenberg-Richter relationship. In other words, the statistical characteristic of earthquakes is considered in accordance with their spatial and temporal distribution. For this purpose, the basic data of fault and seismicity associated with the magnitude of earthquakes are investigated by the distribution of earthquakes and faults. Considering the b-value quantity at any point, the map of differential stress (σ_1-σ_3) for depth sources of less than 20 km and more 20 km are calculated according to MPA (Figures 12 and 13).

5. Discussion and Conclusion

Examining the seismic stress structure from two quantification perspectives (the aim of this study) and its numerical quantity are important topics in seismology. Studies on the numerical quantity of seismic stress in different tectonic areas by Scholz [57] have proven a logical correlation between the seismic parameter (b-Value) and the numeric quantity of the stress parameter. This correlation in the subduction areas shows good adaptation to the age of Slabs (less than 80 million years). On the other hand, the age of the subducting plate is also affected by the mechanism of negative buoyancy (slab tensile force). In the subduction zones, the age and length parameters of the subducting slab are the main parameters. Due to the existence of friction between the plates, the reduction of the tension difference in other parts will not be far from expected. Therefore, at the same time, there is an inverse linear relationship between the b-value and stress in the adjacent continental parts. For this reason, for a more detailed study of the Makran region, it will be essential to investigate the stress structure in terms of numerical quantity.

Based on the study of changes in seismicity parameters in the Makran zone [60] and clustering of large earthquakes that form areas with high-stress concentration, the heterogeneity of seismicity parameters covers a significant part of the study area. Large b-values indicate the random occurrence of small earthquakes, indicating low-stress structures in parts of the region. Heterogeneity of seismic zones leads to changes in the value of b. Based on the seismicity parameters calculated in the Makran zone, the highest concentration of seismic potential for destructive earthquakes with probability is located in the southern terminal of Nehbandan, Bam, Gowk fault systems (connection zones of Nehbandan fault system terminal, Chaman, OrnachNal and Qazband with the thrust faults of Makran zone).

According to the stress fields calculated in the Makran zone, the stress axes mainly rotate locally at depths less than 20 km. The rotation of the maximum seismic stress axis at a depth of less than 20 km is affected by the direction and mechanism of continental crust faults. While the trend of the maximum stress axis in the seismic stress field calculated for a depth of more than 20 km is almost constant and has a northeast-southwest trend and is controlled by the convergence of the tectonic plates in the subduction zone of the Oman plate. The exception in the central part of the Makran zone indicates the interaction of the Makran subduction zone and the Sistan suture.

Acknowledgment

This paper has been prepared based on a research project approved by the International Institute of Earthquake Engineering and Seismology with the number 101/7-A.M.

References

1. Kopp, C., Fruehn, J., Flueh, E.R., Reichert, C., Kukowski, N., Bialas J., and Klaeschen, D. (2000) Structure of the Makran subduction zone from wide-angle and reflection seismic data. *Tectonophysics*, 329, 171-191.

2. Grando, G. and McClay, K. (2007) Morpho-tectonics domains and structural styles in the Makran accretionary prism, offshore Iran. *Sediment. Geol.*, **196**, 157-179.

3. Vernant, Ph., Nilforoushan, F., Hatzfeld, D., Abbasi, M.R., Vigny, C., Masson, F., Nankali, H., Martinod, J. Ashtiani, A., Bayer, R., Tavakoli, F., and Chery, J. (2004) Present-day crustal deformation and plate kinematics in the middle east constrained by GPS measurements in Iran and Northern Oman. *Geophys. J. Int.*, **157**, 381-398.

4. Normand, R., Simpson, G., and Bahroudi, A. (2019) Extension at the coast of the Makran subduction zone (Iran). *Terra Nova*, **31**, 503-510.

5. Vigny, C. Huchon, P. Ruegg, J. Khanbari, K. and M., Asfaw, L. (2006) Confirmation of Arabia plate slow-motion by new GPS data in Yemen. *J. Geophys. Res.*, **111**, B02402, doi:10.1029/2004JB003229.

6. Penney, C., Tavakoli, F., Saadat, A.R., Nankali, H.R., Sedighi, M., Khorrami, F., Sobouti, F., Ra. Z., Cople, A., Jackson, J., and Priestley, K. (2017) Megathrust and accretionary wedge properties and behavior in the Makran subduction zone. *The International Archives of the Photogrammetry, Remote Sensing and Spatial Information Sciences*, **XLII-4/W4**.

7. Stoneley, R. (1974) 'Evolution of the continental margins bounding a former Tethys'. In: Burk, C.A., and Drake, C.L. (Eds.). *The Geology of Continental Margins*. Springer, New York, NY, 889-903.

8. Farhoudi, G. and Karig, D.E. (1977) The Makran of Iran and Pakistan as an active arc system. *Geology*, **5**(11), 664-668.

9. Platt, J.P., Leggett, J.K., and Alam, H.R.S. (1985) Large-scale sediment underplating in the Makran accretionary prism, southwest Pakistan. *Geology*, **13**, 507-511.

10. DeJong, K.A. (1982) *Tectonics of Persian Gulf,*

Gulf of Oman and Southern Pakistan Region. In: Nairn, A.E.M. and Stehli, F.G. (eds) The Indian Ocean. Plenum, New York, 315-351.

11. Kidd, R.G.W. and McCall, G.J.H. (1985) *Plate Tectonics and the Evolution of Makran*. In: McCall, G.J.H. (ed.) East Iran Project, Area No. 1. Geological Survey of Iran, Report, 1, 564-618.

12. White, R.S. (1982) Deformation of the Makran accretionary sediment prism in the Gulf of Oman (Northwest Indian Ocean), in trench-fore arc geology: sedimentation and tectonics on modern and ancient active plate margins, Edited by J.K. Leggett. *Geol. Soc. Spec. Publ.*, **10**, 69-84.

13. Schluter, H.U., Prexl, A., Gaedicke, C., Roeser, H., Reichert, C., Meyer, H., and von Daniels, C. (2002) The Makran accretionary wedge: sediment thicknesses and ages and the origin of mud volcanoes. *Marine Geology*, **185**, 219.

14. Mokhtari, M., Abdoulahi Fard, I., and Hessami, K. (2008) Structural elements of the Makran region, Oman Sea, and their potential relevance to tsunamigenesis. *Natural Hazards*, **47**, 185-199.

15. Kearey, P. and Vine, F.J. (1996) *Global Tectonics*. Second ed. Blackwell Science Ltd., MA, USA.

16. Dolati, A. and Burg, J.-P. (2013) 'Preliminary fault analysis and paleostress evolution in the Makran Fold-and-Thrust Belt in Iran'. In: Al Hosani, K. Roure, F. Ellison, R. and Lokier, S. (Eds.), *Lithosphere dynamics and sedimentary basins: The Arabian Plate and analogues (261-277*). Heidelberg, Germany: Springer. https://doi.org/10.1007/978-3-642-30609-9_13Normand, et al., 2019.

17. Byrne, D.E., Sykes, L.R., and Davis, D.M. (1992) Great thrust earthquakes and aseismic slip along the plate boundary of the Makran Subduction Zone. *J. Geophys. Res.*, **97**(B1), 449-478.

18. Kukowski, N., Schillhorn, T., Flueh, E.R., Huhn, K. (2000) Newly identified strike-slip plate boundary in the northeastern Arabian Sea. *Geology*, **28**(4), 355-358.

19. Okal, E.A. and Synolakis, C.E. (2008) Far-field tsunami hazard from mega-thrust earthquakes in the Indian Ocean. *Geophysical Journal International*, **172**(3), 995-1015.

20. Burg, J.P. (2018) Geology of the onshore Makran accretionary wedge: Synthesis and tectonic interpretation. *Earth-Science Reviews*.

21. Mokhtari, M. et al. (2019) A review of the seismotectonics of the Makran subduction zone as a baseline for Tsunami hazard assessments. *Geoscience Letters*, **6**(13). DOI:10.1186/s40562-019-0143-1 (in Persian).

22. Ellouz-Zimmermann, N. et al. (2007) Offshore frontal part of the Makran Accretionary Prism (Pakistan): the Chamak survey. In: Lacombe O., Lavé J., Roure F., and Vergès J. (eds) *Thrust Belts and Foreland Basins: From Gold Kinematics to Hydrocarbon Systems*. Springer, Berlin, 349-364.

23. Harms, J.C., Cappel, H.N., and Francis, D.C. (1984) 'The Makran coast of Pakistan: its stratigraphy and hydrocarbon potential'. In: *Marine Geology and Oceanography of Arabian Sea and Coastal Pakistan (B.U. Haq and J.D. Milliman, eds)*, 3-27, Van Nostrand Reinhold Co., New York.

24. Leggett, J.K. and Platt, J. (1984) 'Structural features of the Makranfore-arc on Landsat imagery'. In: Haq, B.U., Milliman, J.D. (Eds.), Marine Geology and Oceanography of Arabian Sea and Coastal Pakistan. Van Nostrand Reinhold, New York, 33-43.

25. King, G.C.P., Bilham, R.G., Campbell, J.W., Mckenzie, D.P., and Niazi, M. (1975) Detection of elastic strain field caused by fault creep events in Iran. *Nature*, **253**, 420-423.

26. Agha Nabati, A. (2004) *Geology of Iran*. 586 pages (in Persian).

27. Zarifi, Z. (2006) *Unusual Subduction Zones: Case Studies in Colombia and Iran*. Unpublished Ph.D. Thesis, University of Bergen, Norway.

28. Song, T.R.A. and Simons, M. (2003) Large trench-parallel gravity variations predict seismogenic behavior in subduction zones. *Science*, **301**, 630-633, doi:10.1126/science. 1085557.

29. Wells, R.E., Blakely, R.J., Sugiyama, Y., Scholl, D.W., and Dinterman, P.A. (2003) Basin-centered asperities in great subduction zone earthquakes: A link between slip, subsidence, and subduction erosion?, *J. Geophys. Res.*, **108**(B10), 2507, doi:10.1029/2002JB002072.

30. Hackney, R.I., Echtler, H.P., Franz, G., Gotze, H.J., Lucassen, F., Marchenko, D., Melnick, D., Meyer, U., Schmidt, S., Tasarova, Z., Tassara, A., Wiedecke, S. (2006) 'The segmented overriding plate and coupling at the South-Central Chilean margin (36-42°S)'. In: Oncken, O., Chong, G., Franz, G., Giese, P., Gotze, H.J., Ramos, V.A., Strecker, M.R., Wigger, P. (eds) *The Andes - Active Subduction Orogeny*. Springer, Berlin, 355-374.

31. Pacheco, J.F., Sykes, L.R., and Scholz, C.H. (1993) Nature of seismic coupling along simple plate boundaries of the subduction type. *J. Geophys. Res.*, **98**, 14133-14159.

32. Jacob, K.H. and Quittmeyer, R.L. (1979) 'The Makran region of Pakistan and Iran: Trench-arc system with active plate subduction'. In: Farah, A., de Jong, KA (Eds). *Geodynamics of Pakistan*, 305-317.

33. Seyitoglu, G. Aktug, B., Karadenizli, L., Kaypak, B., Sen, S., Kazanci, N., Isik, V., Esat, K., Parlak, O. Varol, B., Saraç, G., and Ileri, I. (2009) A Late Pliocene - Quaternary pinched crustal wedge in NW Central Anatolia, Turkey: A Neotectonic structure accommodating the internal deformation of the Anatolian plate. *Geological Bulletin of Turkey*, **52**, 121-154.

34. Burchfiel, B.C. and Royden, L.H. (1985) North south extension within the convergent Himalaya region. *Geology*, **13**, 679-682.

35. Frohling, E. and Szeliga, W. (2016) GPS constraints on interplate locking within the Makran subduction zone. *Geophys. J. Int.*, **205**(1), 67-76.

36. Hoffmann, G., Grutzner, C., Reicherter, K., and Preusser, F. (2015) Geo-archaeological evidence for a Holocene extreme flooding event within the Arabian Sea (Ras al Hadd, Oman). *Quat. Sci. Rev.*, 113, 123-133.

37. Lin, N.Y., Jolivet, R., Simons, M., Agram, P.S., Martens, H.R., Li. Z., and Lodi, S.H. (2015) High interseismic coupling in the Eastern Makran (Pakistan) subduction zone. *EPSL*, **420**, 116-126.

38. Pourbeyranvand, S. and Shomali, Z.H. (2012) Determination of stress tensor based on inversion of earthquake focal mechanisms and implementation in Makran region. *Iranian Geophysical Journal* (in Persian), **6**(2), 1-19.

39. Rostam, G.G., Pakzad, M., Noorbakhsh Mirzaei, N., and Sakhaei, S.R. (2018) Analysis of the stress field and strain rate in Zagros-Makran transition zone. *J. Seismol.*, **22**, 287-301.

40. Mehr, H., Asayesh, A.M., and Mokhtari, M. (2018) Splay faults in the Makran subduction zone and changes of their transferred coulomb stress. *Journal of the Earth and Space Physics*, **43**(4), 1-10.

41. Jentzer, M., Fournier, P., Agard, J., Omrani, M., Khatib, M. and Whitechurch, H. (2017) Neogene to present paleostress field in Eastern Iran (Sistan belt) and implications for regional geodynamics. *Tectonics*, **36**, 321-339.

42. Nissen, E., Yamini-Fard, F., Tatar, M., Gholamzadeh, A., Bergman, E. Elliott, J., Jackson, J., and Parsons, B. (2010) The vertical separation of mainshock rupture and micro-seismicity at Qeshm island in the Zagros fold-and-thrust belt, Iran. *Earth Planet. Sci. Lett.*, **296**(3-4), 181-194.

43. Regard, V., Hatzfeld, D., Molinaro, M., Aubourg, C., Bayer, R., Bellier, O., Yamini-Fard, F., Peyret, M. and Abbassi, M. (2010) The transition between Makransubduction and the Zagros collision: recent advances in its structure and active deformation. *Geological Society, London, Special Publications*, **330**, 43-64, https://doi.org/10.1144/SP330.4.

44. Dziewonski, A.M., Chou, T.A., and Woodhouse, J.H. (1981) Determination of earthquake source parameters from waveform data for studies of global and regional seismicity. *J. Geophys. Res.*, **86**, 2825-2852, 1981. doi:10.1029/JB086iB04p02825.

45. Maury, J., Cornet, F.H., and Dorbath, L. (2013) A review of methods for determining stress fields from earthquake focal mechanisms: application to the Sierentz 1980 seismic crisis (Upper Rhine graben). *Bull. Soc. Geol. France*, **184**(4-5), 319-334.

46. Michael, A.J. (1984) Determination of stress from slip data: faults and folds. *J. Geophys. Res.*, **89**, 11517-11526.

47. Gephart, J.W. and Forsyth, D.W. (1984) An improved method for determining the regional stress tensor using earthquake focal mechanism data: application to the San Fernando earthquake sequence. *J. Geophys. Res.*, **89**, 9305-9320.

48. Angelier, J. (2002) Inversion of earthquake focal mechanisms to obtain the seismotectonic stress IV-a newmethod free of choice among nodal lines. *Geophys. J. Int.*, **150**, 588-609.

49. Lund, B. and Slunga, R. (1999) Stress tensor inversion using detailed microearthquake information and stability constraints: application to Olfus in southwest Iceland. *J. Geophys. Res.*, **104**, 14 947-14 964.

50. Hardebeck, J.L. and Michael, A.J. (2006) Damped regional-scale stress inversions: methodology and examples for southern California and the Coalinga aftershock sequence. *J. Geophys. Res.*, **111**, B11310.

51. Arnold, R. and Townend, J. (2007) A bayesian approach to estimating tectonic stress from seismological data. *Geophys. J. Int.*, **170**, 1336-1356.

52. Wallace, R.E. (1951) Geometry of shearing stress and relation to faulting. *J. Geol.*, **59**, 118-130.

53. Bott, M.H.P. (1959) The mechanics of oblique slip faulting. *Geol. Mag.*, **96**, 109-117.

54. Lay, T. and Wallace, T.C. (1995) *Modern Global Seismology*. Academic Press.

55. Michael, A.J. (1987) Use of focal mechanisms to determine stress: a control study. *J. Geophys. Res.*, **92**(B1), 357-368.

56. Spada, M., Tormann, T., Wiemer, S., and Enescu, B., (2013) Generic dependence of the frequency-size distribution of earthquakes on depth and its relation to the strength profile of the crust. *Geophys Res Lett*, **40**, 709-714. https://doi.org/10.1029 /2012GL054198.

57. Scholz, C. H., (2015) On the stress dependence of the earthquake b value. *Geophys Res Lett.*, 42:1399-1402. https://doi.org/10.1002/2014GL062863.

58. Ghorbani, G. R., Pakzad, M., Mirzaei, N., Sakhaei, S. R., (2018) Analysis of the stress field and strain rate in Zagros-Makran transition zone. *J. Seismol.*, **22**, 287-301, doi: 10.1007/s10950-017-9705-x.

59. Regard, V., Hatzfeld, D., Molinaro, M., Aubourg, C., Bayer, R., Bellier, O., Yamini-Fard, F., Peyret, M., and Abbassi, M. (2010) The transition between Makransubduction and the Zagros collision: recent advances in its ?????

60. Mostafazadeh, M. and Mahshadnia,L. (2022) Evaluation of seismic stress change in the Makran zone. *Geophysical Journal of Iran.* **16**(2), 191-205.

Appendix 1. Seismic data used for stress inversion.

Year	Mount	Day	Minute	Second	Y	X	Magnitude	Depth	Azimuth	Dip	Rake	Ref.
1977	1	5	5	44	56.7304	29.00	5.1	29	204	27	98	GCMT
1977	3	21	21	19	56.4444	27.47	6.7	18.8	267	27	98	GCMT
1977	3	21	22	42	56.9697	27.63	6.1	19.3	241	26	78	GCMT
1977	3	22	11	57	56.1300	27.23	5.9	10	75	43	96	GCMT
1977	3	23	23	51	56.4400	27.25	5.5	10	261	41	92	GCMT
1977	4	1	13	36	56.4000	27.37	5.9	10	262	44	90	GCMT
1977	10	19	6	35	55.1200	27.57	5.5	15	117	41	120	GCMT
1977	12	10	5	46	56.7400	27.50	5.6	15	248	9	78	GCMT
1978	3	16	2	0	66.4300	29.83	6.1	39.2	104	77	-173	GCMT
1978	12	10	11	16	66.2000	29.80	5.9	33	101	79	-176	GCMT
1979	1	10	1	26	61.2300	26.75	6	15	338	62	-152	GCMT
1979	1	10	15	5	61.3100	26.75	6.1	15	328	58	-159	GCMT
1980	1	1	2	45	60.2700	26.99	5.5	64	208	80	-178	GCMT
1980	4	28	7	4	64.3300	27.73	5.5	43	39	17	-119	GCMT
1980	11	17	18	26	56.0700	26.98	5.2	15	251	30	87	GCMT
1980	11	28	21	15	56.5691	27.63	5.6	15.1	311	37	134	GCMT
1981	4	16	10	27	56.3971	27.74	5.4	24.6	221	42	18	GCMT
1981	6	11	7	24	57.8569	29.88	6.1	17.7	172	37	171	GCMT
1981	7	28	17	22	57.9191	29.97	6	12.5	150	13	119	GCMT
1983	2	7	15	6	57.6405	26.94	5.6	23.3	5	42	172	GCMT
1983	4	18	10	58	62.1795	27.80	6.5	52.4	81	43	-68	GCMT
1983	7	12	11	34	56.5371	27.62	5.8	22.4	241	45	73	GCMT
1984	1	18	14	8	65.9460	28.01	5.5	14.8	349	50	-13	GCMT
1984	10	2	3	19	66.4500	26.96	5.3	12.6	191	76	0	GCMT
1986	10	16	19	54	66.4500	27.24	5	46.6	1	60	28	GCMT
1987	4	29	1	45	55.9300	26.99	5	15	273	42	114	GCMT
1987	5	12	7	15	55.3200	27.95	5.4	15	278	34	104	GCMT
1987	8	10	10	52	63.7200	29.65	6	157	349	32	-73	GCMT
1987	12	18	16	24	56.4200	27.90	5.8	15	155	39	-149	GCMT
1988	6	9	0	9	56.8365	28.28	5	31	310	11	139	GCMT
1989	4	2	6	42	57.1463	28.10	5.4	29.3	242	24	81	GCMT
1989	11	20	4	19	57.7578	29.85	5.7	17.9	240	75	9	GCMT
1989	12	7	12	59	58.9723	25.95	5.8	12	142	37	103	GCMT
1990	3	4	19	46	66.4381	28.84	5.8	18.1	278	78	-176	GCMT
1990	4	27	5	29	66.4320	28.75	5.4	19.4	358	57	8	GCMT
1990	6	17	4	51	65.7749	27.34	6	15.8	210	63	15	GCMT
1990	6	17	17	17	65.6469	27.33	5.3	15.5	115	56	173	GCMT
1990	7	26	6	54	65.6642	27.34	5.9	28	209	63	2	GCMT
1990	8	14	0	50	66.1471	27.04	5.3	24.6	287	71	-170	GCMT
1990	9	8	19	33	66.2672	27.47	5.7	31.5	197	75	12	GCMT
1990	9	26	15	32	60.5100	29.06	5.6	15	189	90	-180	GCMT
1990	11	6	18	45	55.2500	28.06	6.5	15	274	37	107	GCMT
1990	11	14	18	45	66.2216	27.52	5.4	26.9	97	59	191	GCMT
1991	12	7	14	22	63.0901	25.15	5.2	27	309	8	133	GCMT
1991	12	19	18	55	57.2291	28.02	5.4	41.1	215	35	26	GCMT
1992	1	20	8	58	66.1294	27.50	5.3	27.4	99	72	170	GCMT
1992	1	30	5	22	63.1905	24.96	5.5	28.2	298	10	126	GCMT
1992	4	24	7	7	66.1900	27.52	5.9	25.6	102	60	156	GCMT
1992	5	19	12	24	55.3500	28.05	5.6	15	254	40	99	GCMT
1992	8	28	0	50	66.8755	29.27	5.6	14.8	118	67	179	GCMT
1992	9	11	18	24	60.7705	29.92	5.3	29.2	91	25	51	GCMT
1992	12	17	10	39	61.4886	25.92	5.8	30.4	8	54	142	GCMT

Appendix 1. Continue

Year	Mount	Day	Minute	Second	Y	X	Magnitude	Depth	Azimuth	Dip	Rake	Ref.
1993	4	12	14	0	57.1099	28.21	5.3	27.9	292	44	97	GCMT
1993	7	9	10	29	55.5100	28.45	5.2	23	110	26	120	GCMT
1994	2	23	8	2	60.5884	30.78	6.1	12.8	145	33	96	GCMT
1994	2	23	11	54	60.5595	30.74	5.3	16.4	108	31	62	GCMT
1994	2	24	0	11	60.5190	30.75	6.1	11.4	158	43	105	GCMT
1994	2	26	2	31	60.5873	30.84	5.9	10.2	168	30	92	GCMT
1994	2	28	11	13	60.6480	30.80	5.6	23.5	136	30	92	GCMT
1994	12	10	12	16	65.0690	27.92	5.2	47.3	204	37	-130	GCMT
1996	2	26	8	8	57.0900	28.32	5.5	33	315	7	125	GCMT
1996	10	18	9	26	57.6900	27.26	5.3	15	289	21	83	GCMT
1997	4	19	5	53	57.0100	27.64	5.5	19	215	58	22	GCMT
1997	7	27	23	33	56.5600	27.41	5.4	33	108	76	175	GCMT
1997	10	20	6	9	57.4500	27.98	5.4	33	293	46	119	GCMT
1997	12	4	10	17	64.8100	29.43	5.1	33	53	46	119	GCMT
1998	1	5	16	58	64.6100	29.13	5.1	18	48	37	104	GCMT
1998	3	14	19	40	57.6009	30.11	6.6	26.4	154	57	-174	GCMT
1998	6	10	8	30	58.5200	28.00	5.3	105.6	167	10	-32	GCMT
1998	8	1	23	38	56.5268	27.64	5	22.2	88	42	92	GCMT
1999	1	14	22	12	56.4067	28.94	5.1	27.1	210	44	-57	GCMT
1999	3	4	5	38	57.2579	28.28	6.2	33.4	250	16	68	GCMT
2000	3	5	9	40	56.4000	27.61	5.4	33	290	45	106	GCMT
2001	4	13	1	4	55.0400	27.55	5.1	26.1	166	34	135	GCMT
2001	11	25	21	30	57.0500	27.74	5	29	299	32	135	GCMT
2002	3	11	20	6	55.7700	24.82	5	15	224	32	-103	GCMT
2002	4	17	8	47	56.6725	27.54	5.3	32.8	237	39	36	GCMT
2003	1	14	14	13	62.3965	27.92	5.5	39.7	61	41	-92	GCMT
2003	2	14	10	28	56.8027	27.97	5.3	24	288	18	97	GCMT
2003	6	24	6	52	61.0719	27.33	5.4	42	97	45	-65	GCMT
2003	7	6	16	4	57.5300	27.59	5	33	102	48	7	GCMT
2003	8	4	3	28	59.7988	29.01	5.3	17.8	168	28	117	GCMT
2003	8	21	4	2	59.7880	28.96	5.5	21.5	183	76	-172	GCMT
2003	11	5	7	58	56.1093	27.50	5.2	19.2	70	39	105	GCMT
2003	12	26	1	56	58.3062	28.88	6	18.8	172	59	167	GCMT
2004	1	28	9	6	57.4808	26.96	5.3	25	27	59	161	GCMT
2004	7	22	3	56	65.3600	28.71	5.1	47.5	70	60	-7	GCMT
2004	10	7	12	54	57.3400	28.14	5	12	211	67	-156	GCMT
2004	12	8	10	4	57.3200	27.71	5	58	3	64	162	GCMT
2005	2	22	2	25	56.8061	30.74	6	10.8	71	44	79	GCMT
2005	3	13	3	31	61.9128	27.07	6	50.3	253	37	-89	GCMT
2005	11	27	10	22	55.8000	26.66	5.9	12	257	39	83	GCMT
2005	11	27	11	13	55.5900	26.70	5	14.6	254	49	52	GCMT
2005	11	27	16	30	55.8900	26.65	5.5	12	218	87	-2	GCMT
2006	2	28	7	31	56.9111	28.08	5.8	30.1	302	19	118	GCMT
2006	3	25	7	29	55.6000	27.43	5.9	14	269	28	83	GCMT
2006	3	25	9	55	55.6800	27.48	5.5	12	276	35	89	GCMT
2006	3	25	10	0	55.6600	27.41	5.2	12	267	30	70	GCMT
2006	3	25	11	3	55.6200	27.53	5	12	261	33	59	GCMT
2006	6	3	7	15	55.8300	26.72	5.1	12	111	45	112	GCMT
2006	6	28	21	2	55.8100	26.77	5.8	12	247	33	96	GCMT
2006	7	18	23	27	61.2181	26.27	5.2	41.2	107	67	-12	GCMT
2006	11	7	12	31	64.9943	24.55	5.1	35	137	61	9	GCMT
2007	2	27	22	28	55.2300	27.97	5	22.8	280	42	108	GCMT

Appendix 1. Continue

Year	Mount	Day	Minute	Second	Y	X	Magnitude	Depth	Azimuth	Dip	Rake	Ref.
2007	3	23	21	38	55.1200	27.48	5	12	265	42	69	GCMT
2007	4	25	4	19	56.3400	28.04	5.2	18.6	282	34	94	GCMT
2007	7	24	10	8	56.7400	27.14	5	20.5	270	21	81	GCMT
2007	8	25	4	24	56.7655	28.18	5	31.8	314	85	-178	GCMT
2007	10	19	7	19	66.2241	28.57	5	29.2	197	86	-2	GCMT
2008	9	10	11	0	55.7200	26.65	6.1	12	234	33	76	GCMT
2008	9	17	17	43	55.9600	26.75	5.2	12	245	45	59	GCMT
2008	12	7	13	36	55.7400	26.82	5.4	12	69	41	115	GCMT
2008	12	8	14	41	55.7600	26.83	5.1	12	238	49	59	GCMT
2008	12	9	15	9	55.8000	26.75	5	14	241	33	73	GCMT
2009	2	2	8	36	66.5168	27.18	5	15.2	189	81	-6	GCMT
2009	4	30	10	4	61.4645	27.74	5.6	69.9	21	35	-167	GCMT
2009	5	7	22	44	57.0300	25.16	5.1	25.2	227	26	82	GCMT
2009	5	7	22	44	57.0668	25.42	5.3	29.4	227	26	82	GCMT
2009	7	22	3	53	55.7000	26.60	5.3	12	297	44	91	GCMT
2009	10	25	14	47	64.0900	29.52	5.6	135.7	154	2	22	GCMT
2009	11	3	23	26	56.1600	27.04	5	13.2	246	30	63	GCMT
2010	6	5	16	59	66.0400	27.87	5	22.3	196	83	6	GCMT
2010	7	31	6	52	56.7713	29.55	5.4	11.3	211	60	-25	GCMT
2010	8	14	20	18	66.3100	28.10	5.2	19.9	208	83	-5	GCMT
2010	12	20	18	42	59.1592	28.39	5.9	14.8	36	87	180	GCMT
2011	1	18	20	23	63.9948	28.68	7.2	79.9	77	31	-60	GCMT
2011	1	27	8	38	59.0520	28.15	5.7	18.5	122	64	-29	GCMT
2011	1	28	4	20	58.9400	28.03	5.2	12	133	74	-14	GCMT
2011	3	5	20	42	57.1298	28.28	5.2	27.9	327	5	144	GCMT
2011	6	15	1	5	57.5600	27.71	5.4	41.4	333	45	157	GCMT
2011	6	26	19	46	57.6525	30.03	5	24.8	114	36	71	GCMT
2011	8	10	0	53	65.1363	27.77	5.6	43.6	11	72	-163	GCMT
2012	4	18	17	40	57.9600	27.76	5.1	88.1	76	54	-164	GCMT
2012	12	25	17	36	66.5071	28.40	5	23.6	108	60	160	GCMT
2013	1	21	19	48	57.5182	30.36	5.2	15.2	235	70	13	GCMT
2013	4	16	10	44	62.1360	27.97	7.7	63.1	80	35	-72	GCMT
2013	4	17	3	15	62.3378	28.12	5.7	59.9	82	36	-81	GCMT
2013	5	9	8	1	57.6900	26.51	5	12	256	85	2	GCMT
2013	5	11	2	8	57.8438	26.66	5.8	15.1	346	74	-178	GCMT
2013	5	11	3	41	57.9509	26.61	5	10	249	78	2	GCMT
2013	5	12	0	7	57.7788	26.71	5.5	24	350	63	176	GCMT
2013	5	12	10	54	57.7834	26.73	5.4	14.4	350	66	176	GCMT
2013	5	18	10	3	57.6800	26.50	5.5	12	344	72	179	GCMT
2013	5	18	10	57	57.6400	26.49	5.5	26.49	351	69	178	GCMT
2013	9	24	17	20	65.5461	27.11	5.5	16.1	107	68	175	GCMT
2013	9	24	11	30	65.0421	26.70	7.8	12	223	39	4	GCMT
2013	9	27	18	8	65.5900	27.15	5	20.2	297	87	179	GCMT
2013	9	28	7	34	65.6192	27.16	6.4	18.7	111	59	158	GCMT
2013	10	18	13	12	64.2100	25.81	5.2	16.5	125	72	-173	GCMT
2013	10	18	13	18	66.5526	28.34	5.3	11.7	125	72	-173	GCMT
2013	10	28	19	4	64.1900	25.78	5	18.5	309	70	-162	GCMT
2014	2	2	14	26	57.7799	26.62	5.3	19.3	352	78	-172	GCMT
2014	2	11	0	9	65.4900	26.98	5.1	16.7	111	70	162	GCMT
2014	5	27	5	44	55.7200	26.38	5.3	15.1	112	70	-178	GCMT
2014	6	13	6	17	65.9631	27.69	5.1	19.4	100	46	172	GCMT
2014	7	22	2	31	57.1100	27.54	5	31.2	124	65	-27	GCMT

Appendix 1. Continue

Year	Mount	Day	Minute	Second	Y	X	Magnitude	Depth	Azimuth	Dip	Rake	Ref.
2014	9	25	2	31	65.7772	27.28	5.4	51.1	124	65	-27	GCMT
2014	9	25	6	16	65.8270	27.26	5.1	34.3	216	61	-157	GCMT
2014	10	24	12	38	57.3775	27.76	5.1	23.2	357	37	125	GCMT
2014	11	10	13	52	55.7100	27.75	5.2	15	349	41	180	GCMT
2015	5	4	11	30	61.2300	26.12	5.1	26.1	308	83	4	GCMT
2015	7	15	11	26	65.8900	27.30	5.3	12	47	21	96	GCMT
2015	7	31	10	6	57.6446	30.05	5.1	12.8	156	82	180	GCMT
2015	8	3	13	16	65.9508	27.35	5.4	25.3	41	23	73	GCMT
2015	10	27	13	15	65.9738	27.26	5	25	55	26	90	GCMT
2016	1	22	20	51	55.1800	28.20	5.1	20.8	89	42	113	GCMT
2016	3	21	14	48	66.1300	27.62	5.7	27.6	90	58	-176	GCMT
2016	5	13	7	1	66.4225	30.64	5.3	14.8	111	70	175	GCMT
2017	1	29	8	51	65.9900	26.60	5	12	343	40	-8	GCMT
2017	2	7	22	3	63.2448	25.10	5.9	28.5	249	6	64	GCMT
2017	2	8	11	2	63.2654	25.01	5.1	16.2	300	19	101	GCMT
2017	8	31	1	30	56.8800	27.73	5.4	24.4	98	45	151	GCMT
2017	10	23	0	24	56.9300	27.76	5.4	12	103	45	157	GCMT
2017	12	6	23	41	65.6300	27.23	5.4	12	350	70	-19	GCMT
2018	3	7	14	46	57.5700	27.80	5.2	42.8	313	45	121	GCMT
2018	9	7	6	23	59.4000	28.02	5.6	17.5	114	65	-10	GCMT
2018	11	16	20	17	58.2900	27.95	5	94.3	209	72	-6	GCMT
2019	2	10	10	54	55.5400	26.94	5.5	12	344	76	-178	GCMT
2019	12	30	13	49	56.5000	27.13	5.2	18.3	223	28	41	GCMT